

# Critical polymer–polymer phase separation in ternary solutions

Lei Guo and Erik Luijten\*

Department of Materials Science and Engineering, University of Illinois at Urbana–Champaign,  
1304 West Green Street, Urbana, Illinois 61801, U.S.A.

(Dated: November 20, 2018)

We study polymer–polymer phase separation in a common good solvent by means of Monte Carlo simulations of the bond-fluctuation model. Below a critical, chain-length dependent concentration, no phase separation occurs. For higher concentrations, the critical demixing temperature scales nonlinearly with the total monomer concentration, with a power law relatively close to a renormalization-group prediction based on “blob” scaling arguments. We point out that earlier simulations and experiments have tested this power-law dependence at concentrations outside the validity regime of the scaling arguments. The critical amplitudes of the order parameter and the zero-angle scattering intensity also exhibit chain-length dependences that differ from the conventional predictions but are in excellent agreement with the renormalization-group results. In addition, we characterize the variation of the average coil shape upon phase separation.

PACS numbers: 61.25.Hq, 64.75.+g, 82.35.Lr, 82.60.Lf

## I. INTRODUCTION

Understanding the incompatibility of chemically different polymer species is a topic of great practical importance that consequently has received widespread attention over the last decades. Although a very large number of experiments has been performed—including determination of the coexistence curve<sup>1</sup>, the Flory–Huggins interaction parameter<sup>2,3,4</sup>, and of critical exponents<sup>5,6</sup>—several basic theoretical predictions<sup>7,8,9,10,11,12</sup> have proven difficult to verify, as they rely on specific assumptions, such as monodisperse and symmetric conditions, in which the solvent interacts equally with both polymer species. While, on the other hand, these conditions can easily be realized in computer simulations, those mostly have focused on polymer demixing in binary blends, i.e., at relatively high concentrations (cf. Refs. 13,14). Sariban and Binder<sup>15,16,17</sup> have performed pioneering computational work on polymer–polymer demixing under more dilute conditions, using a simple cubic lattice model. The fact that little additional computational work appears to have been done since then has motivated us to further explore polymer demixing in the presence of a solvent.

Flory–Huggins (FH) theory<sup>7,8</sup> predicts that two incompatible polymer species in a nonselective good solvent will phase separate at arbitrary dilution, provided the temperature of the system is sufficiently low. Under the appropriate conditions, the phase transition will be continuous and the corresponding critical temperature  $T_c$  is predicted to increase linearly with the total monomer concentration  $\phi$  over the entire concentration range. However, this mean-field approach assumes homogeneous monomer densities for both species and ignores the chain connectivity. Below the dilute–semidilute threshold  $\phi^*$ , this connectivity causes individual chains to be separate, swollen coils that do not interpenetrate. Thus, de Gennes<sup>9</sup> has claimed that *no phase separation* occurs for concentrations  $\phi < \phi^*$ . Furthermore, in the semidilute regime,  $\phi > \phi^*$ , each chain can be viewed as a succession of “blobs,” where each blob contains several monomers. In a good solvent, a blob does not contain monomers of other chains due to the excluded-volume interactions. This reduces the number of contacts between monomers of different species and consequently lowers the critical temperature compared to the FH prediction. Specifically, the critical temperature no longer varies linearly with concentration, but decreases superlinearly with decreasing concentration.<sup>9,18</sup> Employing renormalization-group (RG) techniques, Joanny and co-workers<sup>10</sup> observed that demixing under good solvent conditions is driven by corrections to scaling. Schäfer and Kappeler<sup>11</sup> calculated the corresponding spinodal by means of an RG approach and found a nonlinear dependence of the critical temperature on concentration that differs from the prediction of Ref. 18. Broseta *et al.*<sup>12</sup> subsequently extended the RG treatment to predict the chain-length dependences of critical amplitudes of the order parameter, zero-angle scattering intensity and the correlation length. These predictions have partially been tested in Ref. 17, where the concentration dependence of the critical temperature in the semidilute regime and the chain-length dependence of the critical amplitude of the order parameter have been investigated.

In this paper, we extend the work of Ref. 17 by means of Monte Carlo simulations in which we employ the bond-fluctuation model<sup>19,20</sup> rather than a simple cubic lattice model. This model is capable of a more realistic representation of mixtures of flexible chains, as it permits variation of the length of chain segments and a much smoother variation of the angle between successive segments. We investigate phase separation as a function of total monomer concentration and test the various theoretical predictions for the critical properties, where we also address an alternative scenario leading to a nonlinear variation of the transition temperature with concentration. In addition, our simulations explicitly cover the transition from the dilute to the semidilute regime in ternary solutions, which

requires (computationally demanding) calculations in the grand-canonical ensemble. Following our earlier work<sup>21</sup>, we also investigate the effect of this transition on shape properties of individual polymer coils. The shape variation of polymers upon phase separation is of interest because of its influence on the physical properties of ternary solutions. As was first recognized by Kuhn<sup>22</sup>, the shape of a flexible polymer is ellipsoidal rather than spherical. This may affect, e.g., the flow properties of polymeric fluids<sup>23</sup> and the polymer-induced depletion potential in colloid–polymer mixtures.<sup>24</sup> Furthermore, Murat and Kremer<sup>25</sup> proposed a coarse-grained model for the study of phase separation of polymer blends, in which each coil is replaced by a “soft” ellipsoidal particle. Since individual segments are no longer modeled explicitly, this may permit the observation of the demixing process at longer times scales. However, it also requires accurate knowledge of the actual ellipsoidal shape of the individual chains. For polymer chains in the dilute limit, corresponding studies have indeed been performed. Šolc and Stockmayer<sup>26,27</sup> first introduced the radius-of-gyration tensor. The three eigenvalues of this gyration tensor are the squared principal components of the radius of gyration. From Monte Carlo simulations of an ideal polymer chain on a cubic lattice, they found that these three components were very different, implying an asymmetric polymer shape and confirming Kuhn’s original observation. The *asphericity*  $A$  was introduced to characterize the coil shape.<sup>28,29</sup> It takes values between 0 (sphere) and 1 (rod) and was calculated for ideal and self-avoiding chains.<sup>29,30</sup> Since this asphericity does not distinguish prolate-ellipsoid and oblate-ellipsoid shapes, another parameter  $S$  was introduced<sup>29</sup> and calculated analytically for ideal and self-avoiding chains. However, in order to simplify the calculations for  $A$  and  $S$  (both of which are defined below), expectation values of ratios were replaced by ratios of averages. This approximation was found to overestimate the asphericity of polymer chains.<sup>31,32</sup> Numerical calculations<sup>32,33,34</sup> have supported the analytical calculations. In recent years, it has actually become possible to observe the shape asphericity experimentally.<sup>35,36</sup> These experiments, as well as the vast majority of the theoretical work, focus on the shape of a single polymer chain in a highly dilute solution. Studies of the influence of concentration are rare and have essentially shown that the asphericity of athermal chains diminishes only very gradually as a function of increasing concentration.<sup>37,38</sup> In a poor solvent, the reverse effect occurs, due to the coil–globule transition taking place in the polymer-lean phase.<sup>39</sup> The dependence of polymer shape on both concentration and solvent quality has motivated our earlier study of the shape change of polymers upon phase separation in ternary solutions.<sup>21</sup> It was found that phase separation strongly influences the shape of the minority component in a given phase. Here, we expand this work by investigating the temperature dependence of both the asphericity  $A$  and the prolate–oblate parameter  $S$  at fixed total concentration.

## II. THEORETICAL BACKGROUND

Our study consists of three main aspects: (i) The scaling of the critical temperature  $T_c$  with total monomer concentration  $\phi$  and degree of polymerization  $N$ ; (ii) the chain-length dependence of critical amplitudes; (iii) the shape variation of polymers upon phase separation. In this section, we provide the necessary theoretical background and review the corresponding predictions.

### A. Scaling of the critical demixing temperature with concentration and degree of polymerization

We consider a monodisperse solution containing polymers of two different species, denoted A and B, with degree of polymerization  $N_A = N_B = N$ . In addition, the solvent is of the same quality for both species, and their chemical potentials are equal. Thus, a so-called *symmetric* ternary system is realized, in which both species behave identically. The only distinction between monomers of type A and monomers of type B is their mutual repulsion of strength  $\varepsilon_{AB} > 0$ . Identical monomers experience an attraction  $\varepsilon_{AA} = \varepsilon_{BB} < 0$ . Accordingly, phase separation occurs at sufficiently low temperatures. Owing to the symmetric properties of both species, this transition is continuous if the chemical potential difference vanishes. FH theory, assuming complete screening of the excluded-volume interactions, predicts a linear relation between the corresponding critical temperature  $T_c$  and the monomer concentration  $\phi$  (cf. Ref. 8),

$$\frac{\Delta\varepsilon}{k_B T_c} \propto \frac{1}{N} \phi^{-1}, \quad (1)$$

where  $\Delta\varepsilon = (2\varepsilon_{AB} - \varepsilon_{AA} - \varepsilon_{BB})/2$ . Equation (1) implies that polymer–polymer (PP) phase separation occurs for arbitrarily low  $\phi$ , provided that the temperature is sufficiently low. However, in the dilute regime ( $\phi < \phi^*$ ), the excluded-volume interaction is not screened at all and polymer coils essentially do not interact. Accordingly, de Gennes<sup>9,18</sup> argued that no PP phase separation can occur for concentrations below  $\phi^*$ . At the overlap threshold  $\phi^*$  phase separation can be induced, provided that the segregation factor is sufficiently strong (or the temperature sufficiently low). In the semidilute regime ( $\phi > \phi^*$ ), the tendency to phase separate is suppressed as well, and

demixing will take place at a lower temperature than predicted by FH theory, due to the partial screening of the excluded-volume interaction. According to blob scaling arguments<sup>9</sup>, in this regime each chain can be viewed as a succession of blobs. Each blob only contains monomers of a single species, so that the number of A–B contacts is reduced and phase separation is correspondingly suppressed. Indeed, de Gennes has predicted the critical temperature to scale as<sup>9,18</sup>

$$\frac{\Delta\varepsilon}{k_B T_c} \propto \frac{1}{N} \phi^{-\frac{1}{3\nu-1}} \simeq \frac{1}{N} \phi^{-1.31} \quad (\phi > \phi^*). \quad (2)$$

Alternatively, phase separation can be induced by varying the concentration at a fixed temperature  $T$ . At low temperatures, it follows from the previous argument that the total monomer concentration must be increased to  $\phi^*$ . However, if the segregation factor is weak (i.e., at high temperatures), the homogeneous phase persists into the semidilute regime and separation only occurs at a critical concentration

$$\phi_c \propto (T/N)^{3\nu-1} \simeq (T/N)^{0.764} \quad (\phi > \phi^*), \quad (3)$$

where  $\nu = 0.588$  is the scaling exponent for the end-to-end distance  $R$  (or the radius of gyration  $R_g$ ) as a function of  $N$  in dilute solution. We observe that  $\phi_c$  exhibits the same chain-length dependence as the overlap threshold  $\phi^*$ . By contrast, an RG approach<sup>10</sup> indicated that for the fixed point corresponding to phase separation under good solvent conditions, the chemical mismatch between A and B is an *irrelevant parameter*. Indeed, phase separation is predicted to be driven by the *corrections to scaling*. Consequently, the scaling predictions Eqs. (2) and (3) are modified, as shown by an RG calculation of the spinodal.<sup>11</sup> Specifically, it was found that for demixing in the semidilute regime, at a temperature  $T$ , the critical concentration scales as,

$$\phi_c \propto (T/N)^{(3\nu-1)/(1+x)} \simeq (T/N)^{0.624}. \quad (4)$$

From the analogy between a polymer solution and the  $n$ -vector model in the limit  $n \rightarrow 0$ , the exponent  $x$  can be related to the negative of the crossover exponent of the isotropic fixed point of the  $n$ -vector model with cubic anisotropy.<sup>10,12</sup> This crossover exponent has been calculated in a third-order  $\varepsilon$ -expansion<sup>40</sup>, and from a Padé–Borel resummation the value  $x = 0.225$  (5) was obtained.<sup>12</sup> The most notable difference between Eqs. (3) and (4) is that in the RG result the critical concentration (at fixed temperature) decreases with chain length at a slower rate than the overlap threshold  $\phi^* \sim 1/N^{3\nu-1}$ , i.e., for sufficiently long chains (and weak segregation factor) phase separation sets in at higher concentrations than predicted by Eq. (3). For experiments at fixed concentration [cf. Eqs. (1) and (2)], the critical temperature is now given by

$$\frac{\Delta\varepsilon}{k_B T_c} \propto \frac{1}{N} \phi^{-\frac{1+x}{3\nu-1}} \simeq \frac{1}{N} \phi^{-1.60} \quad (\phi > \phi^*). \quad (5)$$

Interestingly, Olvera de la Cruz<sup>41</sup> generalized the work of Ref. 12 to microphase separation in diblock copolymer solutions and predicted that the order–disorder transition temperature  $T_{\text{ODT}}$  exhibits the same concentration dependence as described in Eq. (5). Lodge *et al.*<sup>42</sup> found very good agreement with this prediction for solutions of poly(styrene-*b*-isoprene) (PS-PI) diblock copolymers, whereas the transition temperatures for poly(ethylene-propylene-*b*-ethyl-ethylene) solutions followed a *different* power law. While the results for PS-PI solutions can be viewed as a confirmation of the RG scenario, the agreement between theory and experiment may well be fortuitous, as most data were taken in the concentrated regime where the blob scaling approach is invalid. Guenza and Schweizer<sup>43</sup> subsequently studied the order–disorder transition by means of PRISM theory and observed that local concentration fluctuation effects also imply a nonlinear variation of  $T_{\text{ODT}}$ , resulting from a concentration-dependent local correlation hole affecting the  $\chi$  parameter,

$$\frac{1}{T_{\text{ODT}}} \propto \frac{1}{N} \phi^{-\frac{4\nu-1}{3\nu-1}} \simeq \frac{1}{N} \phi^{-1.77}. \quad (6)$$

Thus, while the integral equation theory cannot quantitatively capture the critical fluctuations that lead to the RG result, it predicts a numerically similar power law that results from a very different mechanism. Unlike the blob scaling arguments, this mechanism explicitly applies to the concentrated solution regime.

## B. Scaling of critical amplitudes with degree of polymerization

Critical properties only exhibit nonclassical scaling behavior within a certain region around the critical point, determined by the Ginzburg criterion.<sup>44</sup> For larger deviations from  $T_c$ , i.e., when  $|t| \gg G$ , where  $t$  is defined as

$(T - T_c)/T_c$  and  $G$  denotes the Ginzburg number, classical or mean-field-like critical exponents are observed (cf. Refs. 45,46). For polymer mixtures, the Ginzburg number decreases as  $1/N$ , so that Ising-like critical exponents are only observed in a very narrow temperature region around the critical point.<sup>47</sup> According to Broseta *et al.*<sup>12</sup>, the modified chain-length dependence of the critical temperature and critical concentration described in Sec II A also affects the Ginzburg criterion, so that the number of blobs per chain  $\tilde{N} \propto (\phi_c/\phi^*)^{1/(3\nu-1)} \sim N^{x/(1+x)}$  replaces  $N$ . Thus, nonclassical behavior is observed within the considerably larger region  $|t|N^{x/(1+x)} \ll 1$ . In addition, the chain-length dependence of all critical amplitudes is modified. In this work, we test these predictions for the order parameter as well as for the zero-angle scattering intensity, for which—to our knowledge—it has not been verified before. In our (semi-)grand-canonical simulations (see Sec. III), the order parameter  $m$  is defined as

$$m = \frac{n_A - n_B}{n_A + n_B}, \quad (7)$$

where  $n_A, n_B$  are the numbers of A and B polymers, respectively. This corresponds to the concentration difference (for either species A or species B) between the A-rich and the B-rich phases. In simulations of finite systems, the ensemble average  $\langle m \rangle$  vanishes<sup>48</sup>, which is resolved by employing the absolute value of the order parameter,  $\langle |m| \rangle$ . For the sake of consistency, we thus phrase the following theoretical expressions in terms of  $\langle |m| \rangle$ . Composition fluctuations are probed via the zero-angle scattering intensity (osmotic compressibility)<sup>49</sup>

$$S_{\text{coll}}(0) = nN\phi(\langle |m|^2 \rangle - \langle |m| \rangle^2) \propto \phi^2 V(\langle |m|^2 \rangle - \langle |m| \rangle^2), \quad (8)$$

where  $n \equiv n_A + n_B$  is the total number of polymers. Near criticality, both  $\langle |m| \rangle$  and  $S_{\text{coll}}(0)$  exhibit a power-law dependence on the reduced temperature  $t$ ,

$$\langle |m| \rangle = \hat{B}(N)|t|^\beta, \quad (9)$$

$$S_{\text{coll}}(0) = \hat{\Gamma}(N)|t|^{-\gamma}, \quad (10)$$

where  $\beta$  and  $\gamma$  denote critical exponents and  $\hat{B}(N)$  and  $\hat{\Gamma}(N)$  are  $N$ -dependent amplitudes. Within the asymptotic scaling region,  $\beta$  and  $\gamma$  assume their Ising values,  $\beta \simeq 0.327$  and  $\gamma \simeq 1.237$ .<sup>50</sup> The chain-length dependence of the amplitudes follows directly from the observation that  $t/G = tN$  constitutes the proper scaling variable and that  $\hat{B}$  and  $\hat{\Gamma}$  must be independent of  $N$  in the mean-field limit. Thus,

$$\hat{B}(N) \propto N^{\beta-1/2} \simeq N^{-0.173}, \quad (11)$$

$$\hat{\Gamma}(N) \propto N \cdot N^{1-\gamma} \simeq N^{0.763}, \quad (12)$$

where  $\hat{\Gamma}(N)$  involves an additional factor  $N$  because of the prefactor in Eq. (8). The revised scaling of  $\hat{B}(N)$  and  $\hat{\Gamma}(N)$  with  $N$  yields<sup>12,17</sup>

$$\hat{B}(N) \propto \tilde{N}^{\beta-1/2} = N^{x(\beta-1/2)/(1+x)} \simeq N^{-0.0318}, \quad (13)$$

$$\hat{\Gamma}(N) \propto N \cdot \tilde{N}^{1-\gamma} = N^{1+x(1-\gamma)/(1+x)} \simeq N^{0.956}. \quad (14)$$

Equation (13) was verified in Ref. 17. It is one of the goals of the present work to test the prediction Eq. (14) for the compressibility and to reproduce the scaling for the order parameter in the context of the bond fluctuation model. A final noteworthy point concerns the so-called Fisher renormalization of critical exponents<sup>51</sup>, which is expected to occur for experiments and simulations at fixed concentration. It has been predicted<sup>12</sup> that for polymer demixing this renormalization occurs within an exceedingly narrow range around the critical temperature, whereas regular Ising-type exponents are predicted to occur outside this range (but within the nonclassical regime predicted by the Ginzburg criterion).

### C. Shape variation of polymer coils upon phase separation

The ellipsoidal shape of a polymer coil is characterized by the eigenvalues  $\lambda_1 \leq \lambda_2 \leq \lambda_3$  of the radius-of-gyration tensor  $\mathbf{Q}$ , which is defined as<sup>27,30</sup>

$$Q_{\alpha\beta} = \frac{1}{2N^2} \sum_{i,j=1}^N [r_{i,\alpha} - r_{j,\alpha}][r_{i,\beta} - r_{j,\beta}], \quad (15)$$

where  $\mathbf{r}_i$  represents the position of the  $i$ th monomer along the chain and  $\alpha, \beta = 1, 2, 3$  denote cartesian components. An important measure is the *asphericity*  $A^{29,31,32,52}$ :

$$A = \frac{1}{2} \left\langle \frac{(\lambda_1 - \lambda_2)^2 + (\lambda_2 - \lambda_3)^2 + (\lambda_3 - \lambda_1)^2}{(\lambda_1 + \lambda_2 + \lambda_3)^2} \right\rangle, \quad (16)$$

which takes values between 0 (sphere) and 1 (rod). In dilute solution it approaches a universal value as  $N \rightarrow \infty$ , estimated as 0.415 from first-order  $\varepsilon$ -expansions and as 0.431 from simulations.<sup>32,34,53</sup> In the melt limit, where the chains behave ideally, this value is anticipated to decrease to the (exactly known) RW value 0.39427...<sup>31</sup> Another measure of the polymer shape is  $S$ ,

$$S = \left\langle \frac{(\lambda_1 - \bar{\lambda})(\lambda_2 - \bar{\lambda})(\lambda_3 - \bar{\lambda})}{\bar{\lambda}^3} \right\rangle, \quad (17)$$

where  $\bar{\lambda}$  is the average value of  $\lambda_1$ ,  $\lambda_2$  and  $\lambda_3$ .  $S$  distinguishes oblate-shaped polymers ( $-\frac{1}{4} < S < 0$ ) from prolate-shaped chains ( $0 < S < 2$ ). In the dilute limit it approaches a universal value 0.541, as estimated from simulations.<sup>32,34</sup> Upon approach of the melt limit it decreases to a value that is estimated as 0.475 from numerical integration<sup>32</sup> and 0.478 from simulations.<sup>32</sup>

### III. SIMULATION MODEL AND DETAILS

The bond fluctuation model (BFM) has been introduced for the Monte Carlo simulation of polymer systems in Refs. 19 and 20. In this lattice model, a chain consists of connected units, each of which occupies a cubic lattice cell. Every unit represents a Kuhn segment corresponding to 3 to 5 real monomers.<sup>54</sup> The units cannot overlap and are connected by bond vectors with lengths between 2 and  $\sqrt{10}$  lattice constants; restricting the vectors to this set prevents the crossing of bonds. Important differences between the BFM and a self-avoiding random-walk (Verdier–Stockmayer<sup>55</sup>) model are the flexibility of the segment length (the distance between two connected units) and the resulting increase in the number of possible bond angles (i.e., the angle between two adjacent segments). Monomer interactions are implemented by means of a square-well potential with a range of  $\sqrt{6}$  lattice constants, which covers 54 out of the 108 possible positions for neighboring segments. The attractive coupling strength between segments of the same species is set to  $\varepsilon_{AA} = \varepsilon_{BB} = -1/k_B T$ . Unlike species repel each other with a strength  $\varepsilon_{AB} = \delta/k_B T$ , where  $\delta > 0$  is a variable parameter. Throughout this paper, units are chosen such that  $k_B = 1$  and temperatures correspond to the inverse coupling constant  $\delta/\varepsilon_{AB} = -1/\varepsilon_{AA}$ . The solvent is represented by empty lattice sites, and the polymer–solvent interaction  $\varepsilon_{AS}$  and the solvent–solvent interaction  $\varepsilon_{SS}$  both vanish.

The ternary system described here can undergo both polymer–polymer (PP) and polymer–solvent (PS) demixing. Although the former typically occurs at a higher temperature than the latter, it follows from the predictions of Sec. II that the PP demixing temperature decreases with decreasing concentration. Indeed, we found that for simulations using the above-mentioned interaction parameters PP demixing is preempted by PS separation near the dilute–semidilute threshold  $\phi^*$ . In order to be able to determine the concentration dependence of the PP demixing temperature, we therefore explicitly suppress PS phase separation in a *subset* of our calculations. The data presented in Sections IV B and IV D (with the exception of Fig. 14) pertain to  $\varepsilon_{AA} = \varepsilon_{BB} = 0$ . This eliminates all attractive interactions and, apart from the excluded-volume interactions, only leaves the A–B repulsion nonzero.

All simulations are performed for symmetric, monodisperse systems ( $N_A = N_B = N$ ) on simple cubic lattices with linear dimension  $L$  and periodic boundary conditions. In order to permit a finite-size scaling analysis for the determination of critical properties, four different values for  $L$  are studied. Most simulations are performed in the semi-grand-canonical ensemble<sup>15</sup>, in which the *total* monomer concentration  $\phi = \phi_A + \phi_B$  is kept constant and only the identity of chains is changed, governed by their interactions in a given configuration as well as their chemical potential difference. The symmetry of the system makes such Monte Carlo moves possible and also guarantees that the critical point will occur for identical chemical potentials. The A–B changes are supplemented by local (translational) segment moves and reptation-like moves. For strong repulsions, polymer demixing occurs upon variation of concentration rather than temperature (this is the predicted demixing near  $\phi = \phi^*$ , see Sec. II A). Therefore, these simulations are carried out in the full grand-canonical ensemble, in which the *total* monomer concentration fluctuates as well. These calculations, which are particularly computationally intensive, are performed using a variant of the recoil-growth scheme.<sup>56,57</sup> The chemical potential of both species is varied, but the chemical potential difference is fixed at zero in order to maintain critical demixing.

In the semi-grand-canonical simulations, all properties are sampled every 50 or 200 sweeps (depending on  $\phi$  and  $T$ ), where a sweep corresponds to a sequence of, on average, three reptation moves per chain, one local move per monomer

TABLE I: Summary of linear system sizes  $L$  studied for different chain lengths  $N$  and concentrations  $\phi$ . Each system contains  $n = \phi L^3/(8N)$  chains.

	$\phi = 0.12$	$\phi = 0.16$	$\phi = 0.20$	$\phi = 0.24$	$\phi = 0.28$	$\phi = 0.32$	$\phi = 0.40$
$N = 10$			20, 40, 60, 80	30, 40, 50, 60	20, 40, 60, 80	30, 40, 50, 60	20, 30, 40, 50
$N = 20$	40, 60, 80, 100	40, 60, 80, 100	40, 60, 80, 100	40, 60, 80, 100	40, 60, 80, 100	40, 60, 80, 100	
$N = 40$	60, 80, 100, 120	60, 80, 100, 120	40, 60, 80, 100	40, 60, 80, 100	40, 60, 80, 100	40, 60, 80, 100	

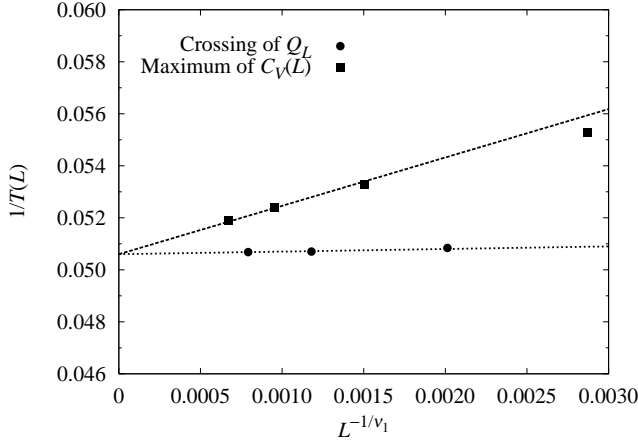


FIG. 1: Finite-size scaling behavior of the characteristic temperatures  $T(L)$  determined from crossing points of the fourth-order amplitude ratio  $Q_L$  and from maxima of the specific heat  $C_V$ . Data apply to a ternary polymer solution with chain length  $N = 20$ , total monomer concentration  $\phi = 0.32$  and repulsion parameter  $\delta = 1$ . Both cases extrapolate to virtually identical estimates for the critical demixing temperature  $T_c$ .

and a semi-grand-canonical move for one quarter of all chains. After equilibration, which comprises 4 000 samples, 100 000 samples are obtained for each state point. For the grand-canonical simulations, properties are sampled every sweep, which corresponds to 200 attempts to insert or delete a polymer chain followed by a semi-grand-canonical move for half of all the chains. In this case, equilibration corresponds to 500 sweeps and each production run to 20 000 to 60 000 sweeps. The data are analyzed by means of multiple-histogram reweighting.<sup>58</sup> For the semi-grand-canonical data only temperature reweighting is performed, whereas the grand-canonical data also permit reweighting with respect to the total monomer concentration (cf. Figs. 3a and 4).

#### IV. SIMULATION RESULTS

##### A. Scaling of the critical demixing temperature in semidilute solutions

In order to determine the critical properties, we first locate the critical temperature  $T_c$  for the polymer–polymer phase separation, as a function of concentration  $\phi$  and chain length  $N$ . For  $N = 10, 20$  and  $40$  we have simulated cubic cells containing up to 1792, 2000 and 750 chains, respectively. Table I lists the system sizes and concentrations employed. We locate  $T_c$  by means of the finite-size scaling properties of the fourth-order amplitude ratio  $Q_L$ <sup>59</sup>,

$$Q_L = \langle m^2 \rangle^2 / \langle m^4 \rangle \quad (18)$$

and the specific heat  $C_V(L)$ ,

$$C_V(L) = (\langle E^2 \rangle - \langle E \rangle^2) / k_B T^2. \quad (19)$$

For each pair of system sizes  $L_1$  and  $L_2$ , the curves for  $Q_L$  as a function of temperature exhibit a crossing point that defines a characteristic temperature  $T_Q(L)$ , where we choose  $L = (L_1 + L_2)/2$ . Likewise,  $C_V(L)$  exhibits a maximum at a temperature  $T_C(L)$ . Both characteristic temperatures approach the critical temperature in the thermodynamic limit. Figure 1 illustrates this for a typical system with  $N = 20$ ,  $\phi = 0.32$  and  $\delta = 1$ . In this figure, we also exploit

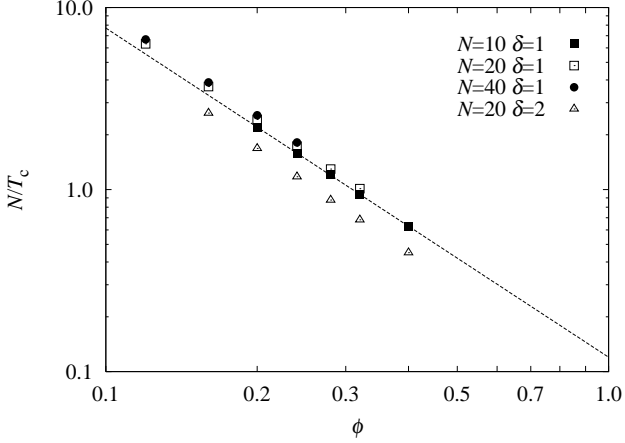


FIG. 2: Scaling of the inverse critical demixing temperature  $N/T_c$  with concentration  $\phi$ , plotted on a double-logarithmic scale. The line, which represents a fit to the data for  $N = 10$ , describes a power-law dependence  $T_c \propto \phi^{-1.808}$ . The open triangles refer to data for a stronger repulsion  $\delta$  between unlike monomers and hence lie at systematically higher temperatures.

the theoretically predicted leading finite-size scaling behavior of the characteristic temperatures,

$$\frac{1}{T(L)} = \frac{1}{T_c} + \frac{D}{L^{1/\nu_1}}, \quad L \rightarrow \infty, \quad (20)$$

where the coefficient  $D$  is nonuniversal and also depends on the thermodynamic property for which  $T(L)$  is determined.  $\nu_1$  denotes the critical exponent for the correlation length and takes the Ising value 0.630.<sup>50</sup> Extrapolation of  $T_Q(L)$  and  $T_C(L)$  using Eq. (20) yields virtually identical estimates for  $T_c$ .

Having obtained the critical temperatures for the 15 cases listed in Table I, we investigate their scaling with chain length and concentration. As shown in Fig. 2, for fixed chain length and monomer repulsion  $\delta$ , the inverse critical temperatures exhibit a power-law dependence on  $\phi$ ,

$$\frac{N}{T_c} \propto \frac{1}{\phi^k}. \quad (21)$$

The results for  $N = 10$  can be described by an exponent  $k = 1.808$  (5), whereas least-square fits for  $N = 20$  and  $N = 40$  lead to  $k = 1.870$  (3) and  $k = 1.880$  (4), respectively. This clearly refutes the mean-field result Eq. (1), according to which  $T_c$  increases linearly with concentration ( $k = 1$ ). On the other hand, we note that our result also shows a stronger variation with  $\phi$  than the nonlinear relation Eq. (5). The blob-scaling arguments underlying the theoretical prediction rely on the assumption that the radius of each blob scales as  $n_{\text{blob}}^\nu$ , where  $n_{\text{blob}}$  is the number of monomers in a single blob. It would have been surprising if this scaling behavior would be obeyed for the rather short chain lengths employed here, which necessarily contain only few, relatively small blobs. In particular, for small blobs the excluded-volume interactions are partially screened, reducing the magnitude of the effective exponent  $\nu_{\text{eff}}$ . Indeed, the observed values for  $k = 1.80\text{--}1.88$  would correspond to an effective blob scaling exponent  $\nu_{\text{eff}} = 0.55\text{--}0.56$ , i.e., only a rather small deviation from  $\nu = 0.588$ . However, we note that our findings are *also* compatible with the alternative expression Eq. (6) for an effective scaling exponent  $\nu_{\text{eff}} = 0.54\text{--}0.57$ .

Interestingly, Sariban *et al.*<sup>17</sup>, employing short chains and a simple cubic lattice model, appear to have found excellent agreement with a power law  $k = 1.60$ , precisely matching the blob-scaling result Eq. (5). Careful examination of Fig. 9 in Ref. 17, however, shows that all data that support this scaling result were obtained for high monomer concentrations,  $\phi = 0.40, 0.60, 0.80$  and chain lengths  $N \leq 32$ . For such concentrated solutions, the blob scaling arguments certainly do not apply, casting a doubt on the origin of the observed power-law behavior. Inclusion of the data for  $\phi = 0.20$  leads to exponents that are significantly larger in magnitude. We note that even for the same value of the scaling variable employed in Ref. 17 [ $N\phi^{1/(3\nu-1)}$ ], the data for the longest chains ( $N = 64$ ) lead to a power law that differs appreciably from  $k = 1.60$ . This brings the observations in Ref. 17 considerably closer to our data for the bond fluctuation model. All data certainly appear consistent with a slow approach of the predicted limiting behavior Eq. (5), but it also cannot be excluded that *simultaneously* an alternative mechanism<sup>43</sup> applies that leads to a rather comparable power-law behavior in the concentrated solution regime.

Another aspect in Fig. 2 is the dependence of the critical demixing temperature on the chain length. Although the plotted data for  $\delta = 1$ , in which  $T_c$  is scaled by  $N$ , do not exactly coincide, the remaining chain length dependence is

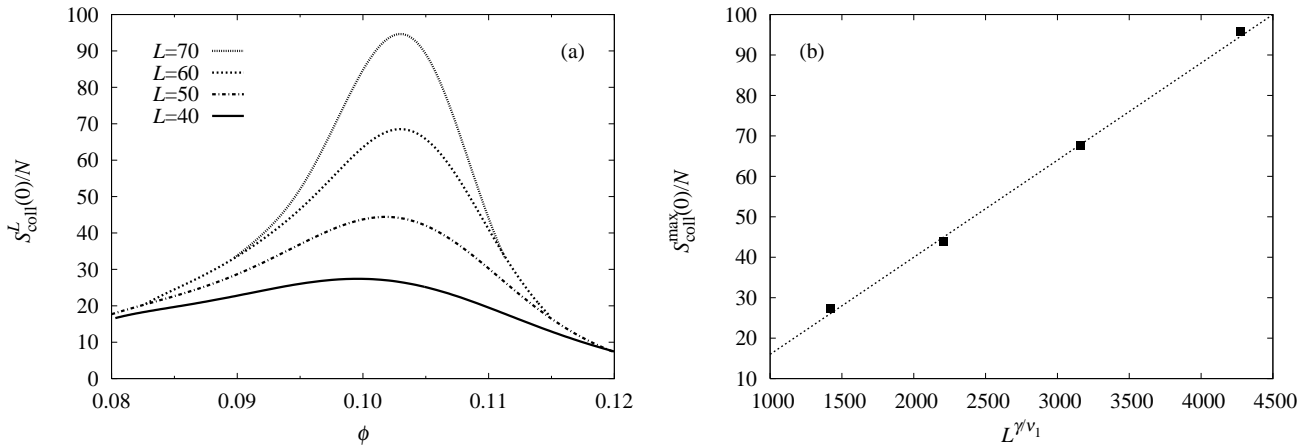


FIG. 3: (a) Zero-angle scattering intensity  $S_{\text{coll}}(0)$  (scaled by the chain length  $N$ ) as a function of monomer concentration  $\phi$  for a ternary solution containing two polymer species with degree of polymerization  $N = 20$ . The data are obtained from grand-canonical simulations at fixed (reduced) temperature  $T = 0.05$ . Away from the maximum the data for different linear system sizes  $L$  converge rapidly, whereas the maximum itself exhibits strong finite-size effects. (b) The height of the maximum increases with system size as  $L^{\gamma/\nu_1} \simeq L^{1.96}$ , where  $\gamma$  and  $\nu_1$  are critical exponents belonging to the Ising universality class.<sup>50</sup> This confirms the occurrence of a critical phase transition as a function of  $\phi$ . As discussed in the text, polymer–solvent separation is suppressed by eliminating attractive interactions between monomers of the same species,  $\varepsilon_{\text{AA}} = \varepsilon_{\text{BB}} = 0$ .

weak and suggestive of an additive small- $N$  correction that vanishes in the limit  $N \rightarrow \infty$ . In order to show the effect of the A–B repulsion on  $T_c$ , we also include data for  $\delta = 2$  for  $N = 20$ . These results exhibit the same power-law dependence on concentration, but phase separation occurs at systematically higher temperatures than for  $\delta = 1$ , as expected from the stronger A–B repulsion.

### B. Polymer–polymer phase separation and the role of the dilute–semidilute threshold

According to FH theory<sup>7,8</sup>, PP phase separation occurs at arbitrarily low concentration. On the other hand, de Gennes<sup>9,18</sup> has predicted that dilute solutions ( $\phi < \phi^*$ ) exhibit no phase separation, whereas a critical demixing transition takes place for symmetric systems if the A–B repulsion is strong enough (or temperature sufficiently low).

In order to test this scenario, we consider a ternary solution with  $N_A = N_B = N = 20$  at very low, fixed temperature  $T = 0.05$  (strong repulsion regime). We perform simulations in the grand-canonical ensemble at several chemical potentials that correspond to a range in monomer concentration and we specifically monitor the zero-angle scattering intensity  $S_{\text{coll}}(0)$ , Eq. (8), and the fourth-order amplitude ratio  $Q_L$ , Eq. (18). Since the simulations are carried out for four different system sizes,  $L = 40, 50, 60, 70$ , a critical transition will manifest itself via finite-size effects. The compressibility will exhibit a maximum that increases with system size according to a well-defined power law and the amplitude ratio will exhibit a universal crossing point. The compressibility data shown in Fig. 3a, which were obtained by means of histogram reweighting, exhibit precisely this behavior. For each system size,  $S_{\text{coll}}(0)$  displays a maximum  $S_{\text{coll}}^{\text{max}}(0)$  as a function of monomer concentration. This maximum scales with  $L$  as  $L^{\gamma/\nu_1} \simeq L^{1.96}$  (Fig. 3b). The power law is characteristic for the compressibility at a critical phase transition with a one-component order parameter. We note that these simulations are performed at very low temperatures. Nevertheless, phase separation only occurs when a certain critical concentration has been reached. The fourth-order amplitude ratio of moments of the order-parameter distribution confirms these observations. As shown in Fig. 4, the curves for  $Q_L$  for different system sizes exhibit a crossing point at a concentration that is close to the concentration of maximum compressibility (Fig. 3a). The crossing curves are very similar to those commonly employed to determine critical temperatures; the curves for successive system sizes do not all cross at a single concentration owing to finite-size corrections. However, it is noteworthy that the value of  $Q_L$  at the crossing point approaches the universal Ising value  $Q_L = 0.6233$  (cf. Ref. 50) with increasing  $L$ .

Table II lists the critical concentration  $\phi_c$  determined from both the compressibility and the fourth-order amplitude ratio for chain lengths 10, 20, and 40. As an alternative approach, we exploit the notion that, at fixed concentration  $\phi$ , the curves for  $Q_L(T)$  for two different system sizes  $L$  must exhibit a crossing point, if the system undergoes phase separation. Thus, if such a crossing point is observed,  $\phi \geq \phi_c$  and if no crossing point can be detected,  $\phi < \phi_c$ .

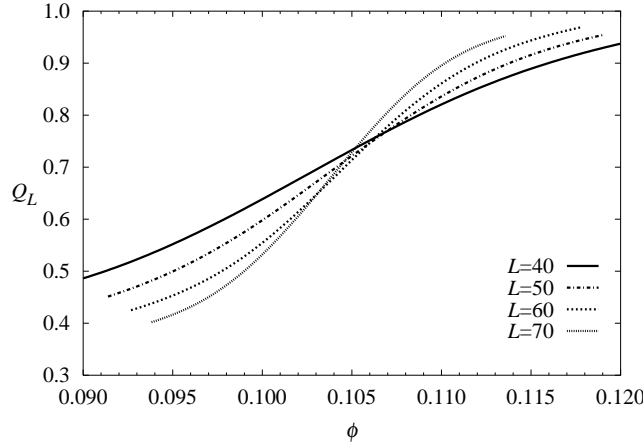


FIG. 4: Fourth-order amplitude ratio  $Q_L$  as a function of monomer concentration for different system sizes  $L$ . The data pertain to the system described in the caption of Fig. 3. The crossing points, which occur near the location of the compressibility maxima in Fig. 3a, approach the concentration at which critical polymer–polymer demixing takes place.

TABLE II: Critical concentration for phase separation at low temperatures (strong segregation factor).  $\phi_c$  is determined from extrapolation of the maxima of the compressibility and of the crossing points of the fourth-order amplitude ratio  $Q_L$  (cf. Figs. 3 and 4).  $\tilde{\phi}$  is determined by detecting whether, at fixed concentration, two curves for  $Q_L$  exhibit a crossing point at some temperature.

$N$	$\phi_c$	$\tilde{\phi}$
10	$0.131 \pm 0.005$	$0.13375 \pm 0.00125$
20	$0.101 \pm 0.005$	$0.10375 \pm 0.00125$
40	$0.077 \pm 0.003$	$0.07625 \pm 0.00125$

The resulting estimates ( $\tilde{\phi}$  in Table II) indeed agree reasonably well with those for  $\phi_c$ . Since the second method is computationally more efficient, we have used it to estimate the critical concentration for chain lengths as large as  $N = 320$ , see Fig. 5.

According to de Gennes<sup>9</sup>, in a good solvent the overlap threshold scales as

$$\phi^* \propto N/R_g^3 \propto N^{1-3\nu} = N^{-0.764}, \quad (22)$$

and for the low-temperature regime  $\phi_c$  is predicted to follow the same scaling behavior. Our findings for  $\phi_c$  (Fig. 5) exhibit a slowly varying, effective power-law behavior, which for the longest chains approaches  $\phi_c \propto N^{-0.50}$ . It is well possible that the trend in the effective exponent continues and reaches the behavior predicted in Eq. (22). We note that the analysis of Broseta *et al.*<sup>12</sup>, which modifies the scaling of  $\phi_c$  from Eq. (3) to Eq. (4), only appears to apply to the semidilute regime. This would imply different scaling behavior for the weak and the strong segregation regimes, and it is therefore not entirely clear whether de Gennes' original prediction for the low-temperature regime ( $\phi_c \simeq \phi^*$ ) indeed remains unaltered.

Finally, the critical concentrations for the low-temperature regime can be combined with the results for the systems listed in Table I to assemble a phase diagram showing the critical lines for three different chain lengths in the concentration–temperature plane, see Fig. 6. The critical lines in the semidilute regime are terminated by the lines labeled  $\phi^*$ . These cutoff lines are drawn vertically to reflect the observation that in this model  $\phi^*$  is insensitive to temperature variation.

### C. Critical amplitudes in ternary solutions

Near a critical point, finite-size scaling theory implies

$$\langle |m| \rangle L^{\beta/\nu_1} = \tilde{f}(tL^{1/\nu_1}) \quad (23)$$

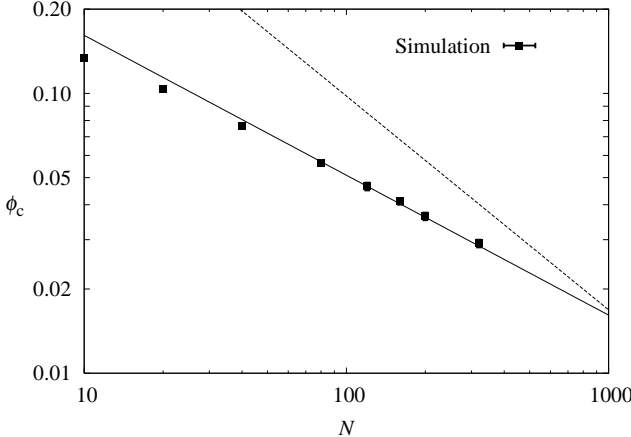


FIG. 5: Scaling of the critical concentration  $\phi_c$  with  $N$  on a log–log scale. All results pertain to a system with  $\varepsilon_{AA} = \varepsilon_{BB} = 0$  in the strong segregation regime ( $1/T = 20$ ). The estimates for  $N > 40$  were obtained from the detection of crossing curves for  $Q_L(T)$ , as explained in the text (cf.  $\tilde{\phi}$  in Table II). The dashed line represents the theoretical prediction that the critical concentration in the strong segregation regime is proportional to the overlap threshold. The solid line represents the effective power-law behavior observed for the longest chains investigated in this work ( $120 \leq N \leq 320$ ).

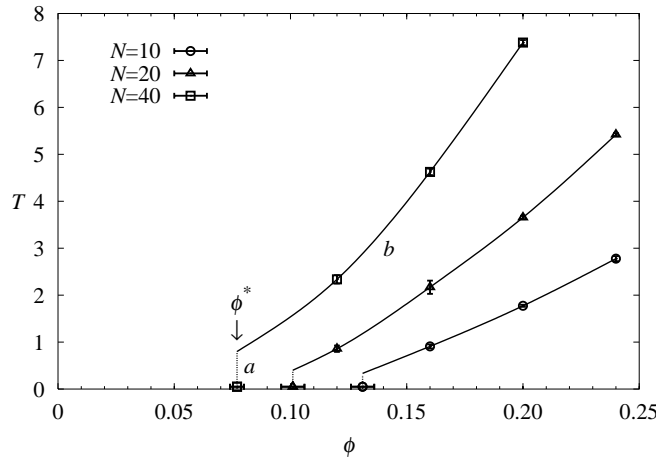


FIG. 6: Phase diagram for polymer–polymer separation as a function of total monomer concentration and temperature, for different  $N$ . All data pertain to systems without monomer attractions,  $\varepsilon_{AA} = \varepsilon_{BB} = 0$ , and hence differ from those presented in Fig. 2. The curves (which are drawn as guides to the eye) separate the mixing region (left-hand side) from the demixing region (right-hand side). The curve  $b$  indicates the weak segregation regime, in which phase separation occurs at high concentrations, whereas the dotted line  $a$  reflects the strong segregation regime where phase separation takes place for concentrations above the overlap threshold. (For clarity, only the curves for  $N = 40$  are labeled.)

and

$$S_{\text{coll}}(0)L^{-\gamma/\nu_1}/\phi^2 = \tilde{S}(tL^{1/\nu_1}), \quad (24)$$

where  $\tilde{f}$  and  $\tilde{S}$  are universal scaling functions.<sup>60</sup> In the finite-size scaling limit,  $tL^{1/\nu_1} \ll 1$ , these equations yield the finite-size scaling behavior at the critical point, commonly employed for the numerical determination of critical exponents.<sup>50</sup> Outside the finite-size scaling regime,  $tL^{1/\nu_1} \gg 1$ , but still sufficiently close to the critical temperature to be within the scaling regime  $t \ll 1$ , the scaling functions reproduce the critical behavior in the thermodynamic limit, i.e.,  $\tilde{f}(x) \sim x^\beta$  and  $\tilde{S}(x) \sim x^{-\gamma}$ . Here, we focus on this second regime. Assuming Ising values for the exponents, we plot  $\langle |m| \rangle L^{\beta/\nu_1}$  in Fig. 7 as a function of  $|t|L^{1/\nu_1}$  for a solution with  $N = 40$  and total concentration  $\phi = 0.24$ . For this system, which has a critical temperature  $T_c = 22.0$  (1), two sets of data are plotted, obtained at  $T = 18.182$  and  $T = 20.000$ , respectively. Each set contains four different system sizes  $L$ , and all data turn out to collapse on a

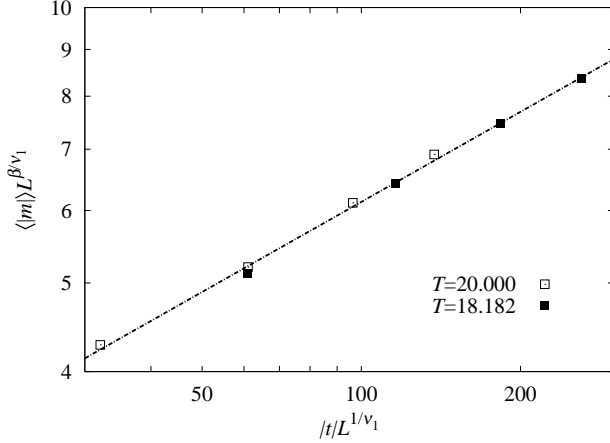


FIG. 7: Finite-size scaling of the demixing order parameter  $\langle|m|\rangle$  for a solution with  $\phi = 0.24$  and  $N = 40$ , near its critical temperature  $T_c = 22.0$  (1). The two data sets pertain to temperatures  $T = 18.182$  and  $T = 20.000$ , respectively. For each temperature, the data points correspond to system sizes  $L = 40, 60, 80$ , and  $100$ . All points are described by a single power law ( $|t|L^{1/\nu_1})^\beta$ , with  $\beta = 0.327$ .

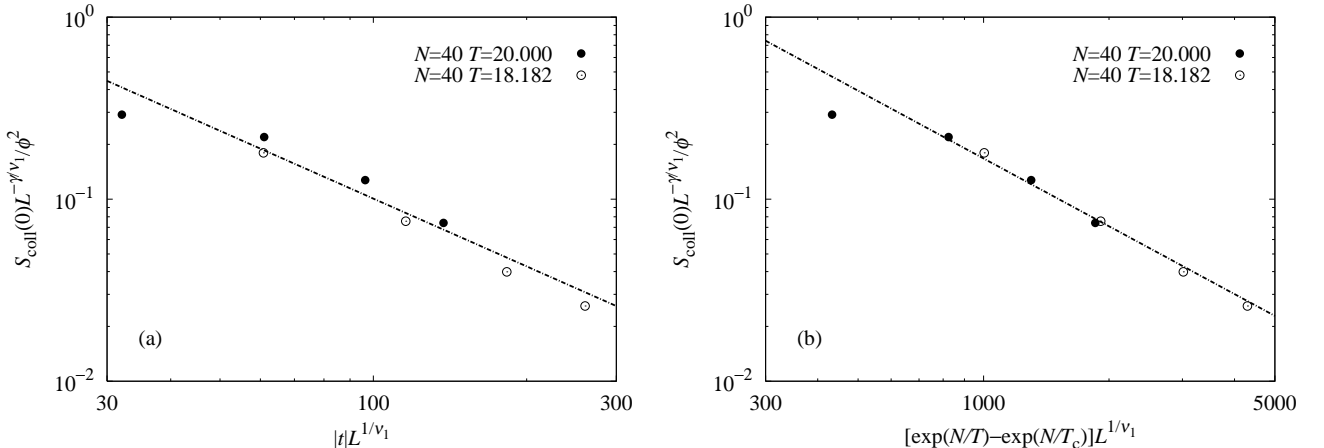


FIG. 8: Finite-size scaling behavior of the zero-angle scattering intensity  $S_{\text{coll}}(0)/\phi^2$  for the system described in the caption of Fig. 7. Panel (a) employs the regular reduced temperature  $|(T - T_c)/T_c|$ , which does not permit a description of all data by a single power law, presumably because of corrections to scaling. In panel (b), the alternative temperature variable  $[\exp(N/T) - \exp(N/T_c)]$  is used, which indeed greatly improves the data collapse and permits the description of all data by a single power law ( $|t|L^{1/\nu_1})^{-\gamma}$ , with  $\gamma = 1.237$ ). The left-most data point in panel (b) deviates because of finite-size corrections.

single line which, on this double-logarithmic scale, has a slope 0.327, the critical exponent  $\beta$  in the Ising universality class. This confirms Eq. (23) and our assumption of Ising exponents. Likewise, data for the zero-angle scattering intensity  $S_{\text{coll}}/\phi^2$  are plotted in Fig. 8a. The data do not fall onto a single curve as well as the data for the order parameter do, which can possibly be ascribed to the fact that the reduced temperature for our data is relatively large and hence corrections to scaling start to become important. Therefore, we replot the same data in Fig. 8b as a function of an alternative temperature variable  $[\exp(N/T) - \exp(N/T_c)]$ , proposed in Ref. 15. To leading order, this variable equals  $-[(N/T_c)\exp(N/T_c)]t$ . Note that, as implied by Eq. (21), the prefactor is independent of  $N$ . This variable indeed improves the scaling behavior and the data in Fig. 8b are well described by a power law  $(tL^{1/\nu_1})^{-\gamma}$ , with  $\gamma = 1.237$ . Similar scaling analyses have been carried for our results for  $N = 10$  and  $N = 20$  (not shown).

By combining the data for different chain lengths, we can test the modified scaling of  $\hat{B}(N)$  and  $\hat{\Gamma}(N)$  with  $N$  as proposed by Broseta, i.e., Eqs. (13) and (14). Figure 9 constitutes the counterpart of Fig. 7, displaying the scaling of the order parameter  $\langle|m|\rangle$  outside the finite-size scaling regime (but within the critical region). In Fig. 9a, the conventional scaling with  $N$  is adopted, in which the reduced temperature  $t$  is replaced by  $tN \propto t/G$  and  $\langle|m|\rangle$  is

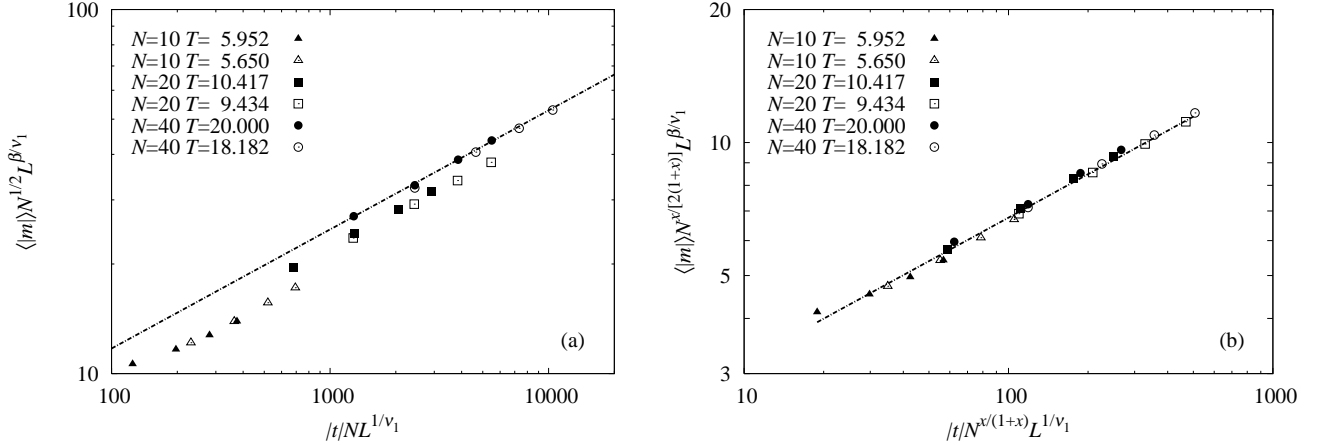


FIG. 9: Scaling of the near-critical order parameter  $\langle |m| \rangle$  with system size  $L$  and degree of polymerization  $N$ . Panel (a) demonstrates that the conventional scaling [Eq. (11)] is not applicable in the semidilute regime. In panel (b), a modified scaling of the critical amplitude is adopted [Eq. (13)], which leads to an excellent collapse of all data points onto a single power law with Ising exponent  $\beta = 0.327$ . Data points pertain to the following systems (all at concentration  $\phi = 0.24$ ): (i)  $N = 10$  ( $T_c = 6.309$ ):  $T = 5.952$  and  $T = 5.650$ . For each temperature, system sizes  $L = 30, 40, 50$ , and  $60$  are employed. (ii)  $N = 20$  ( $T_c = 11.547$ ):  $T = 10.417$  and  $T = 9.434$ . For each temperature, system sizes  $L = 40, 60, 80$ , and  $100$  are employed. (iii)  $N = 40$  ( $T_c = 22.0$ ):  $T = 20.000$  and  $T = 18.182$ . For each temperature, system sizes  $L = 40, 60, 80$ , and  $100$  are employed.

multiplied by  $N^{1/2}$ , following Eq. (11). Evidently, this does not properly describe the scaling of the critical amplitude with the degree of polymerization. However, replacing  $N$  by  $N^{x/(1+x)}$ , i.e., plotting  $\langle |m| \rangle N^{x/[2(1+x)]} L^{\beta/\nu_1}$  as a function of  $|t| N^{x/(1+x)} L^{1/\nu_1}$  (Fig. 9b) leads to an excellent collapse of all data points onto a single line that describes a power law with exponent  $\beta = 0.327$ . Thus, the order parameter scales as

$$\langle |m| \rangle N^{x/[2(1+x)]} L^{\beta/\nu_1} \propto \left[ |t| N^{x/(1+x)} L^{1/\nu_1} \right]^\beta, \quad (25)$$

which can be simplified to

$$\langle |m| \rangle \propto N^{x(\beta-0.5)/(1+x)} t^\beta, \quad (26)$$

in agreement with Eq. (13).

In a similar fashion we test Eq. (14). Based upon Fig. 8 we use the modified reduced temperature  $[\exp(N/T) - \exp(N/T_c)]$  instead of  $-t$ , which does not affect the scaling with  $N$ . Since all data points apply to the same concentration, we investigate the scaling of  $S_{\text{coll}}(0)/(\phi N)$ . Figure 10 demonstrates that all data points except for those with the smallest values of  $|t| L^{1/\nu_1}$  (which cross over to a horizontal line representing the critical finite-size amplitude) are described by a power law with exponent  $-\gamma = -1.237$ . Thus, the following scaling behavior is recovered,

$$\frac{S_{\text{coll}}(0)}{\phi N} L^{-\gamma/\nu_1} N^{-x/(1+x)} \propto \left[ |t| L^{1/\nu_1} N^{x/(1+x)} \right]^{-\gamma} \quad (27)$$

which can be simplified to

$$\frac{S_{\text{coll}}(0)}{\phi N} \propto N^{x(1-\gamma)/(1+x)} t^{-\gamma}, \quad (28)$$

consistent with Eq. (14).

Thus, we conclude that the chain-length dependence of the critical amplitudes in the semidilute regime can *not* be described by the conventional scaling laws, but that the modified scaling behavior proposed by Broseta *et al.*<sup>12</sup> provides an excellent description already for relatively short chains.

#### D. Shape variation of polymers upon polymer–polymer phase separation

In our earlier communication<sup>21</sup>, we studied the shape change of polymers upon phase separation in terms of the *asphericity*  $A$  (see Eq. (16)). We confined ourselves to isothermal variation of the concentration in the strong

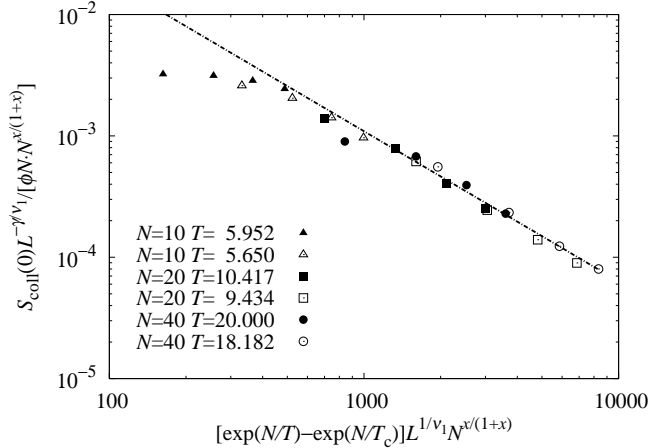


FIG. 10: Scaling of the zero-angle scattering intensity near criticality. Data are assembled for all systems listed in the caption of Fig. 9. Except for some data points that cross over into the finite-size scaling regime (left-hand side of the plot), all data are described by a single power law with exponent  $-1.237$ . This confirms the modified scaling with degree of polymerization, see Eq. (14).

segregation regime, i.e., phase separation near  $\phi = \phi^*$ . This corresponds to an isotherm that intersects the line  $a$  in Fig. 6. Along such an isotherm, the asphericity of the majority component in a given phase decreases merely slightly at sufficiently high concentration due to the screening of the excluded-volume interactions (thus, the shape of a coil becomes slightly more spherical upon increase of the concentration). By contrast, the minority component in each phase exhibits a strong variation of the asphericity. Since a typical coil belonging to the minority species is surrounded by polymers of the majority species, the strong repulsion “squeezes” the minority coil to a much more spherical shape, as confirmed by a rapid drop in  $A$  for the minority polymers. Here, we extend this work by studying other regions of the phase diagram, namely (i) variation of the total monomer concentration at higher temperatures (such that phase separation takes place in the semidilute regime) and (ii) temperature variation at fixed concentration (for  $\phi > \phi^*$ ), where we can also verify any influence of attractions between monomers of the same species (in Ref. 21, such interactions were explicitly ruled out, in order to prevent polymer–solvent phase separation near the overlap concentration). In addition, we extend our analysis of coil shapes by means of the parameter  $S$  [Eq. (17)], which distinguishes between prolate-ellipsoidal and oblate-ellipsoidal shapes.

Figure 11a shows the variation of  $A$  for a symmetric mixture with  $N = 20$  along the  $T = 2.14$  isotherm, which crosses the critical line in the semidilute regime (cf. Fig. 6). Just as observed for the strong segregation regime<sup>21</sup>, the asphericity for the majority component decreases slowly while for the minority component it drops rapidly. The location of the bifurcation in  $A$  is in good agreement with the corresponding critical concentration  $\phi_c$  in Fig. 6. The nature of the aspherical shape is characterized further by the variation of the oblate–prolate parameter  $S$  over this concentration range (Fig. 11b). As the concentration increases in the dilute regime, the coil shape becomes less prolate, until the concentration has reached its critical value and phase separation occurs. Beyond  $\phi_c$ , the minority component (e.g., a chain of type B in the A-rich phase) then becomes less prolate at an even higher rate. On the other hand, the majority component becomes *less spherical* and *more prolate* immediately after phase separation. As explained in Ref. 21, we ascribe this to the diminished repulsion that a typical majority chain experiences in a homogeneous (unmixed) phase. Although the concentration dependence of  $A$  and  $S$  is very similar, there are significant differences in the probability distributions for these quantities. While the distributions for  $A$  are relatively broad<sup>21</sup>, the distributions for  $S$ , both for the majority component (Fig. 12a) and for the minority component (Fig. 12b) exhibit a sharp peak at zero (spherical shape). For the majority component the distribution, including the peak, exhibits only minor variation with concentration in the dilute regime and remains virtually unchanged for  $\phi > \phi_c$ . However, for the minority component the most significant changes in the distribution, including a significant sharpening of the peak, occur for concentrations in the unmixed regime  $\phi \gtrsim 0.16$ . For both components, the distributions provide insight into the relative occurrence of various coil shapes, which can also be oblate-ellipsoidal ( $S < 0$ ).

As evident from the phase diagram (Fig. 6), phase separation can also be induced by lowering the temperature at fixed concentration. The resulting variation in coil shape is illustrated in Fig. 13 for a system with  $N = 20$  and  $\phi = 0.16$ . A bifurcation similar to Fig. 11a is observed, at a temperature that agrees with the critical temperature along the corresponding isochore in Fig. 6. Unlike the behavior upon variation of the concentration, the asphericity of the majority component now remains constant in the unmixed phase. Since the concentration is constant, the screening of

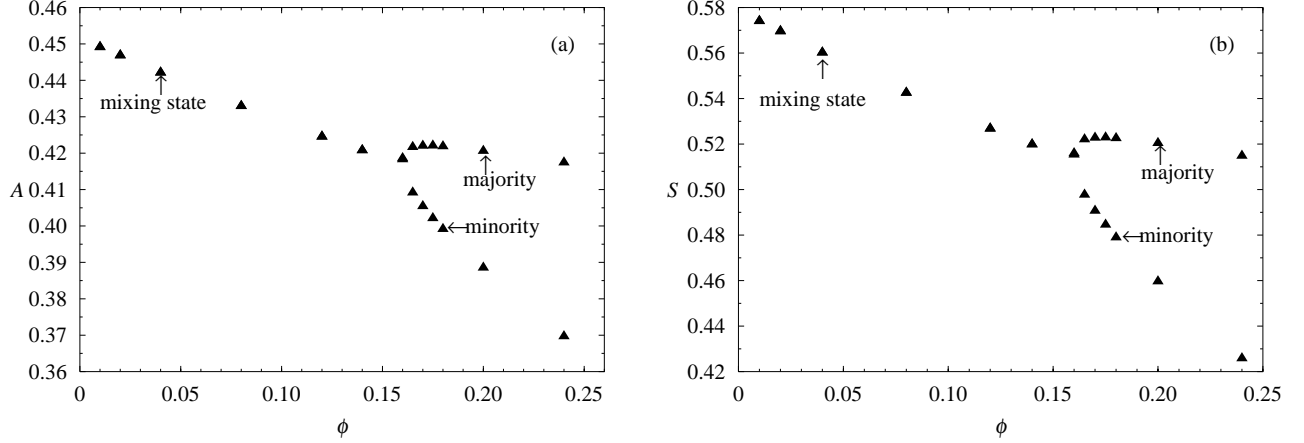


FIG. 11: Characterization of the coil shape in a ternary solution, as a function of monomer concentration  $\phi$ . The temperature is fixed at  $T = 2.14$  and the results pertain to a symmetric mixture with chain length  $N = 20$ . Phase separation occurs near  $\phi = 0.16$  and is driven purely by repulsions between unlike monomers ( $\varepsilon_{AA} = \varepsilon_{BB} = 0$ ). (a) The asphericity  $A$  [Eq. (16)] decreases with increasing concentration, in particular for the minority component, indicating that the coils take an increasingly spherical shape. (b) The oblate–prolate parameter  $S$  [Eq. (17)] demonstrates that the coils have a prolate shape over the entire concentration range. The “elongated” shape is most pronounced in the dilute regime.

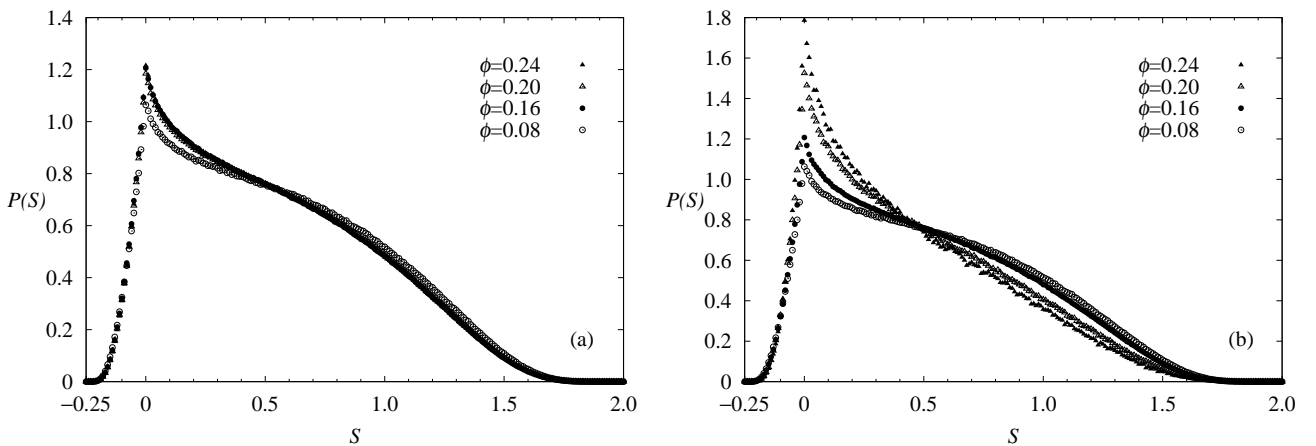


FIG. 12: Probability distribution of the oblate–prolate parameter  $S$  of (a) the majority component and (b) the minority component for different concentrations  $\phi$ , at  $T = 2.14$  for  $N = 20$ . All data pertain to  $\varepsilon_{AA} = \varepsilon_{BB} = 0$ . While the majority component exhibits a virtually invariant distribution for concentrations in the demixed regime  $\phi \gtrsim 0.16$ , the minority component shows a significant sharpening of the peak at  $S = 0$ , which corresponds to a spherical coil shape.

the excluded-volume interactions remains unchanged, and the chains only become somewhat more aspherical as phase separation continues, owing to the diminishing repulsion from the minority component. Since all attractions between monomers of the same species have been set to zero, the majority component finds itself, once phase separation is complete, essentially in an athermal one-component solution.

The effect of attractions between monomers of the same species is addressed in Fig. 14, for a system with  $\varepsilon_{AA} = \varepsilon_{BB} = -1/T$ . The overall behavior of the asphericity is very similar to that displayed in Fig. 11a, with a small, systematic lowering of the asphericity in the dilute regime, induced by the mutual attractions. Thus, the results presented above (Figs. 11 and 12) and in Ref. 21 are not qualitatively affected by the absence of monomer–monomer attractions.

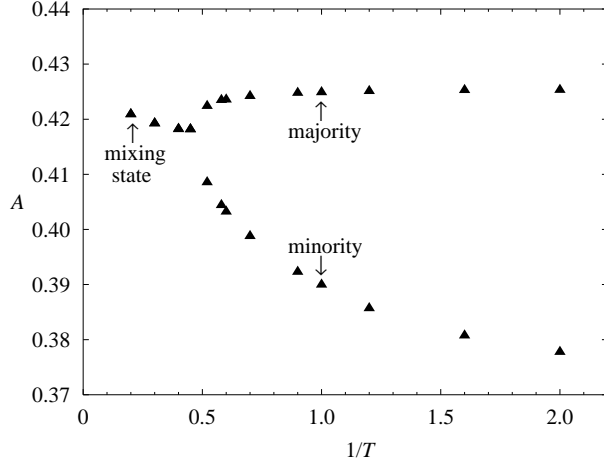


FIG. 13: Variation of the asphericity as a function of inverse temperature for fixed concentration  $\phi = 0.16$ . The results pertain to a system with  $N = 20$  and  $\varepsilon_{AA} = \varepsilon_{BB} = 0$ . Once phase separation is complete (i.e., at low temperature) the majority component is essentially in an athermal one-component solution.

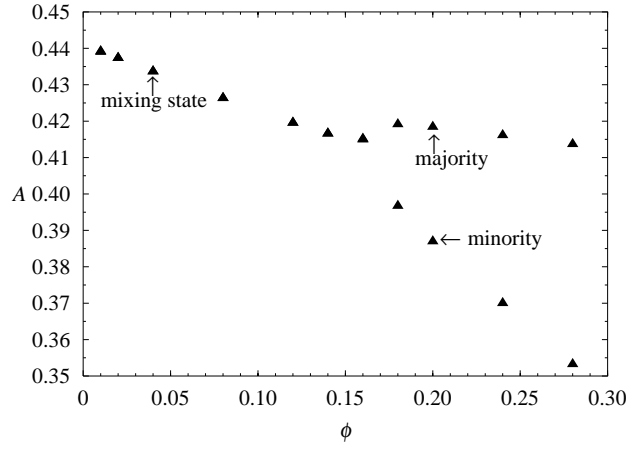


FIG. 14: Asphericity  $A$  as a function of concentration for systems with an explicit, temperature-dependent attraction between monomers of the same species,  $\varepsilon_{AA} = \varepsilon_{BB} = -1/T$ . Chain length is set to  $N = 20$  and temperature to  $T = 5.39$ . This confirms that the absence of A–A and B–B attractions does not qualitatively affect the results presented in Figs. 11 and 12.

## V. CONCLUSIONS

We have studied polymer–polymer phase separation in a common (nonselective) good solvent by means of Monte Carlo simulations of the bond fluctuation model. Our calculations cover both dilute and semidilute solutions, making it possible to distinguish critical demixing in the weak and strong segregation regimes. In the weak segregation regime we have determined the nonlinear concentration dependence of the critical temperature by means of semi-grand-canonical simulations and in the strong segregation regime, where phase separation occurs upon variation of total monomer concentration rather than temperature, by means of grand-canonical simulations. We observed a sudden drop in critical temperature near the overlap threshold, as first predicted by de Gennes<sup>18</sup>, although the chain-length dependence of the corresponding critical concentration differed rather strongly from that expected for the overlap concentration. Also the nonlinear relation between critical temperature and critical concentration in the semidilute regime exhibited a power law that differs from the theoretical prediction<sup>11,12</sup>, which we ascribe to finite chain-length effects. However, it is also possible that, for more concentrated solutions, similar nonlinear behavior results from a concentration dependence of the local correlation hole.<sup>43</sup> This may aid in explaining earlier numerical results<sup>17</sup> and experiments on diblock copolymer solutions<sup>42</sup>, although there are also quantitative differences between those results

and the prediction of Ref. 43. The modified chain-length dependence of all critical amplitudes, first predicted by Broseta *et al.*<sup>12</sup> using a renormalization-group approach, has been verified explicitly for the demixing order parameter and, for the first time, for the zero-angle scattering intensity (osmotic compressibility), whereas a scenario in which the critical amplitudes retain their unmodified chain-length dependence can be convincingly ruled out. The observation of unrenormalized critical exponents is consistent with the prediction that Fisher renormalization of those exponents only takes place within a very narrow temperature range around the critical temperature. Conversely, the observation of nonclassical critical exponents within a rather large temperature range is consistent with a modified Ginzburg criterion<sup>12</sup>, which implies a slow crossover to classical critical exponents.

In a preliminary report<sup>21</sup>, we observed that phase separation causes polymer coils belonging to the minority component to become more spherical, due to repulsion from the surrounding polymers of the opposite species. Here, we have recovered this behavior for more general monomer–monomer interactions and for simulations in which phase separation occurs in the weak segregation regime, as well as for the situation in which phase separation is induced by means of temperature variation rather than variation of the total monomer concentration. In addition, we have characterized the shape variation more precisely by means of the distribution of the prolate–oblate parameter.

### Acknowledgments

This work is supported by the American Chemical Society Petroleum Research Fund under Grant No. 38543-G7 and by the National Science Foundation through an ITR grant (DMR-03-25939) via the Materials Computation Center at the University of Illinois at Urbana-Champaign. E.L. thanks Kurt Binder for drawing his attention to polymer–polymer separation in ternary solutions and Ken Schweizer for pointing out the connection with diblock copolymer solutions. The authors thank Intel for a generous equipment donation and M. Müller for providing parts of the simulation code. The recoil-growth code was originally developed with support of a postdoctoral Fellowship from the Max Planck Institute for Polymer Research and with support of the European Commission through TMR Grant No. ERB FMGE CT950051 for a TRACS visit to the Edinburgh Parallel Computing Centre.

- 
- \* Corresponding author. E-mail: luijten@uiuc.edu
- <sup>1</sup> M. W. J. van den Esker and A. Vrij, *J. Polym. Sci. Polym. Phys. Ed.* **14**, 1943 (1976).
  - <sup>2</sup> T. Fukuda, M. Nagata, and H. Inagaki, *Macromolecules* **17**, 548 (1984).
  - <sup>3</sup> T. Fukuda, M. Nagata, and H. Inagaki, *Macromolecules* **19**, 1411 (1986).
  - <sup>4</sup> M. S. Kent, M. Tirrell, and T. P. Lodge, *Macromolecules* **25**, 5383 (1992).
  - <sup>5</sup> N. Miyashita and T. Nose, *Macromolecules* **28**, 4433 (1995).
  - <sup>6</sup> D. Schwahn, H. Frielinghaus, and L. Willner, *J. Chem. Phys.* **116**, 2229 (2002).
  - <sup>7</sup> R. L. Scott, *J. Chem. Phys.* **17**, 279 (1949).
  - <sup>8</sup> P. J. Flory, *Principles of Polymer Chemistry* (Cornell University Press, Ithaca, N.Y., 1953).
  - <sup>9</sup> P.-G. de Gennes, *Scaling Concepts in Polymer Physics* (Cornell University Press, Ithaca, N.Y., 1979).
  - <sup>10</sup> J. F. Joanny, L. Leibler, and R. Ball, *J. Chem. Phys.* **81**, 4640 (1984).
  - <sup>11</sup> L. Schäfer and C. Kappeler, *J. Phys. (France)* **46**, 1853 (1985).
  - <sup>12</sup> D. Broseta, L. Leibler, and J.-F. Joanny, *Macromolecules* **20**, 1935 (1987).
  - <sup>13</sup> H.-P. Deutsch and K. Binder, *Macromolecules* **25**, 6214 (1992).
  - <sup>14</sup> H.-P. Deutsch and K. Binder, *J. Phys. II (France)* **3**, 1049 (1993).
  - <sup>15</sup> A. Sariban and K. Binder, *J. Chem. Phys.* **86**, 5859 (1987).
  - <sup>16</sup> A. Sariban and K. Binder, *Macromolecules* **21**, 711 (1988).
  - <sup>17</sup> A. Sariban and K. Binder, *J. Colloid Polym. Sci.* **272**, 1474 (1994).
  - <sup>18</sup> P. G. de Gennes, *J. Polym. Sci. Polym. Phys. Ed.* **16**, 1883 (1978).
  - <sup>19</sup> I. Carmesin and K. Kremer, *Macromolecules* **21**, 2819 (1988).
  - <sup>20</sup> H.-P. Deutsch and K. Binder, *J. Chem. Phys.* **94**, 2294 (1991).
  - <sup>21</sup> L. Guo and E. Luijten, *Macromolecules* **36**, 8201 (2003).
  - <sup>22</sup> W. Kuhn, *Kolloid-Z.* **68**, 2 (1934).
  - <sup>23</sup> F. H. Abernathy, J. R. Bertschy, R. W. Chin, and D. E. Keyes, *J. Rheology* **24**, 647 (1980).
  - <sup>24</sup> M. Triantafillou and R. D. Kamien, *Phys. Rev. E* **59**, 5621 (1999).
  - <sup>25</sup> M. Murat and K. Kremer, *J. Chem. Phys.* **108**, 4340 (1998).
  - <sup>26</sup> K. Šolc and W. H. Stockmayer, *J. Chem. Phys.* **54**, 2756 (1971).
  - <sup>27</sup> K. Šolc, *J. Chem. Phys.* **55**, 335 (1971).
  - <sup>28</sup> D. N. Theodorou and U. W. Suter, *Macromolecules* **18**, 1206 (1985).
  - <sup>29</sup> J. A. Aronovitz and D. R. Nelson, *J. Phys. (France)* **47**, 1445 (1986).
  - <sup>30</sup> J. Rudnick and G. Gaspari, *J. Phys. A* **19**, L191 (1986).

- <sup>31</sup> H. W. Diehl and E. Eisenriegler, *J. Phys. A* **22**, L87 (1989).
- <sup>32</sup> O. Jagodzinski, E. Eisenriegler, and K. Kremer, *J. Phys. I (France)* **2**, 2243 (1992).
- <sup>33</sup> M. Bishop and C. J. Saltiel, *J. Chem. Phys.* **85**, 6728 (1986).
- <sup>34</sup> J. W. Cannon, J. A. Aronovitz, and P. Goldbart, *J. Phys. I (France)* **1**, 629 (1991).
- <sup>35</sup> C. Haber, S. A. Ruiz, and D. Wirtz, *Proc. Natl. Acad. Sci. U.S.A.* **97**, 10792 (2000).
- <sup>36</sup> B. Maier and J. O. Rädler, *Macromolecules* **34**, 5723 (2001).
- <sup>37</sup> M. Bishop, D. Ceperley, H. L. Frisch, and M. H. Kalos, *J. Chem. Phys.* **72**, 3228 (1980).
- <sup>38</sup> O. F. Olaj, T. Petrik, and G. Zifferer, *Macromol. Theory Simul.* **6**, 1277 (1997).
- <sup>39</sup> I. Szleifer, *J. Chem. Phys.* **92**, 6940 (1990).
- <sup>40</sup> I. J. Ketley and D. J. Wallace, *J. Phys. A* **6**, 1667 (1973).
- <sup>41</sup> M. Olvera de la Cruz, *J. Chem. Phys.* **90**, 1995 (1989).
- <sup>42</sup> T. P. Lodge, C. Pan, X. Jin, Z. Liu, J. Zhao, W. W. Maurer, and F. S. Bates, *J. Polym. Sci. Polym. Phys. Ed.* **33**, 2289 (1995).
- <sup>43</sup> M. Guenza and K. S. Schweizer, *Macromolecules* **30**, 4205 (1997).
- <sup>44</sup> V. L. Ginzburg, *Sov. Phys. Sol. State* **2**, 1824 (1960).
- <sup>45</sup> E. Luijten and K. Binder, *Phys. Rev. E* **58**, R4060 (1998); also **59**, 7254(E) (1999).
- <sup>46</sup> E. Luijten, *Phys. Rev. E* **59**, 4997 (1999).
- <sup>47</sup> P. G. de Gennes, *J. Physique Lett.* **38**, L441 (1977).
- <sup>48</sup> K. Binder and E. Luijten, *Phys. Rep.* **344**, 179 (2001).
- <sup>49</sup> T. L. Hill, *Statistical Mechanics: Principles and Selected Applications* (McGraw-Hill, New York, 1956).
- <sup>50</sup> H. W. Blöte, E. Luijten, and J. R. Heringa, *J. Phys. A* **28**, 6289 (1995).
- <sup>51</sup> M. E. Fisher, *Phys. Rev.* **176**, 257 (1968).
- <sup>52</sup> G. Gaspari, J. Rudnick, and A. Beldjenna, *J. Phys. A* **20**, 3393 (1987).
- <sup>53</sup> M. Bishop and C. J. Saltiel, *J. Chem. Phys.* **88**, 6594 (1988).
- <sup>54</sup> V. Tries, W. Paul, J. Baschnagel, and K. Binder, *J. Chem. Phys.* **106**, 738 (1997).
- <sup>55</sup> P. H. Verdier and W. H. Stockmayer, *J. Chem. Phys.* **36**, 227 (1962).
- <sup>56</sup> S. Consta, N. B. Wilding, D. Frenkel, and Z. Alexandrowicz, *J. Chem. Phys.* **110**, 3220 (1999).
- <sup>57</sup> E. Luijten, N. B. Wilding, and L. Guo, in preparation.
- <sup>58</sup> A. M. Ferrenberg and R. H. Swendsen, *Phys. Rev. Lett.* **63**, 1195 (1989).
- <sup>59</sup> K. Binder, *Z. Phys. B* **43**, 119 (1981).
- <sup>60</sup> The factor  $\phi^2$  was divided out on the basis of Eq. (8). Since we test the finite-size scaling behavior, Eq. (24), for data at fixed concentration, this factor is immaterial in the present context.